Wire-feed laser additive manufacturing of dissimilar metals via dual molten pool interface interlocking mechanism

HE Yi[1], ZHANG XiaoHan[1], ZHAO Zhe[1], XU ShuoHeng[1], XIA Min[3], ZHANG Chen[1*] & HU YaoWu[1,2*]

[1]The Institute of Technological Sciences, Wuhan University, Wuhan 430072, China;
[2]School of Power and Mechanical Engineering, Wuhan University, Wuhan 430072, China;
[3]Department of Engineering, Lancaster University, Lancaster, LA1 4YW, United Kingdom

Intermetallic compounds produced in laser additive manufacturing are the main factors restricting the joint performance of dissimilar metals. To solve this problem, a dual molten pool interface interlocking mechanism was proposed in this study. Based on a dual molten pool interface interlocking mechanism, the dissimilar metals, aluminum alloy and stainless steel, were produced as single-layer and multilayer samples, using the wire-feed laser additive manufacturing directed energy deposition technology. The preferred parameters for the dual molten pool interface interlocking mechanism process of the dissimilar metals, aluminum alloy and stainless steel, were obtained. The matching relationship between the interface connection of dissimilar metals and the process parameters was established. The results demonstrated excellent mechanical occlusion at the connection interface and no apparent intermetallic compound layer. Good feature size and high microhardness were observed under a laser power of 660 W, a wire feeding speed of 55 mm/s, and a platform moving speed of 10 mm/s. Molecular dynamics simulations demonstrated a faster rate of aluminum diffusion in the aluminum alloy substrate to stainless steel under the action of the initial contact force than without the initial contact force. Thus, the dual molten pool interface interlocking mechanism can effectively reduce the intermetallic compound layer when dissimilar metals are connected in the aerospace field.

laser additive manufacturing, dissimilar metals, dual molten pool interface interlocking mechanism, interface connection, process parameters

1 Introduction

Traditional joining techniques, such as mechanical joining [1,2], friction stir welding [3,4], and laser welding [5,6], are limited by the size of the components and can only be used in components having simple structures. Laser additive manufacturing (LAM) directed energy deposition techniques [7–9] use a laser as a heat source to form a small molten pool on the surface of a substrate with material pre-deposited or supplied in powder or wire form. Thus, size constraints can

be solved, and the formation and growth of intermetallic compounds (IMCs) can be controlled by changing the process parameters (i.e., heat input) to reduce fabrication defects and improve the performance of joints. Therefore, LAM directed energy deposition technology has been widely used as an advanced manufacturing technology in aerospace and other manufacturing fields [10,11]. Wire-feed LAM can be deposited layer by layer along a predesigned trajectory, eventually producing the required components. Wire-feed LAM is becoming the primary additive method for manufacturing large-sized parts because of its advantage of un-limited-forming size [12,13]. Wire-feed LAM [14,15] has

*Corresponding authors (email: c.zhang@whu.edu.cn; yaowuhu@whu.edu.cn)

higher material use, higher deposition rate, lower material cost, and less pollution [16,17] compared to powder-feed LAM [18,19].

Under the "peak carbon dioxide emissions and carbon neutrality" aim, aluminum alloy and steel combinations were selected as dissimilar metals based on the position and function of aircraft parts to achieve lightweight structural parts in the aerospace field [20]. Therefore, it is important to study dissimilar-metal connection methods of aluminum alloy and steel used in aerospace, which can reduce the weight and cost. The metallurgical compatibility during welding, the brittle metal compound formed by the interface reaction, and the difference in the thermal expansion coefficient can affect the connection performance because of the large differences in thermal physical parameters (melting point, thermal expansion coefficient, thermal conductivity, and density) between the aluminum alloy and steel. A large amount of thermal stress can be generated at the joints of aluminum alloy and steel during the welding process. Furthermore, intermetallic brittle compounds are easily formed, resulting in cracks and other damage to the weld [21–24]. The main problem in existing joining processes is that IMCs produced during welding reduce joint strength [25–27]. Therefore, the reduction or inhibition of the formation of IMCs is important for improving the ability of dissimilar metals to connect.

The existing methods to reduce IMCs are primarily by adding a transition layer or filler wire to avoid direct contact between dissimilar metals [28]; this method introduces transition elements such as Cu [29,30], Ni [31,32], Nb [33,34], and V [35,36]. However, this generates more interfaces, and the process is complicated with high manufacturing costs. Thus, it is necessary to examine wire-feed LAM of dissimilar metals, e.g., aluminum alloy and stainless steel, to reduce the generation of several IMC layers by a simple and effective method. Accordingly, this study reports a dual molten pool interface interlocking mechanism (DMPIIM) by using wire-feed LAM directed energy deposition technology. This method is primarily aimed at dissimilar metals with large differences in melting points, and it can avoid direct contact between liquid stainless steel and liquid aluminum alloy by producing a dual molten pool. The proposed DMPIIM does not require the introduction of transition elements. The IMC layer can be reduced; the manufacturing is convenient and relatively inexpensive.

In this study, the dissimilar-metal LAM process was divided into four cases based on the interface connection and a DMPIIM. This study examined the matching relationship between the interfacial connection of a dissimilar couple of aluminum alloy and stainless steel and process parameters such as laser power, wire-feed speed, and platform moving speed. The interfacial connection and element distribution of single-layer molten tracks in different cases were analyzed using a high-speed camera, a three-dimensional (3D) laser profiler, scanning electron microscopy (SEM), and energy dispersive spectroscopy (EDS). The formation of phases was analyzed using X-ray diffraction (XRD). Microhardness was used to characterize the dissimilar-metal interfaces. A 3D numerical model of the interaction between dissimilar metals was established to predict heat and mass transfer. The effects of the initial contact force on the interfacial connection between dissimilar metals aluminum alloy and stainless steel, were examined using molecular dynamics simulations.

2 Experimental

Figure 1(a) shows a schematic of the wire-feed LAM directed energy deposition technique used in this study. The experimental device included a 1-kW continuous wave fiber laser (Shenzhen Maxphotonics Co., Ltd., China). An additive manufacturing process was performed in an Ar atmosphere with a flow rate of 10 L/min. A wire feeder (BWT16) was used for wire feeding. A computer-controlled three-axis computerized numerical control moving platform was used to move the substrate. The angle between the wire and substrate material was between 35° and 75°. An initial contact force was applied to the wire and substrate to ensure good interfacial contact between the dissimilar metals. The force was modulated using an external sensor. Figure 1(b) shows single-layer and multilayer samples processed by DMPIIM wire-feed LAM directed energy deposition technology. Figure 1(c) shows the microscopic characterization of the single-layer sample (laser power of 660 W, wire-feed speed of 55 mm/s, and the platform moving speed of 10 mm/s).

The DMPIIM is a two-molten pool formed by the melting point difference between the wire and substrate (Figure 1 (d)). One molten pool is a wire with a high melting point, and the other is the substrate that is melted by heat transfer through the melting of the wire. The non-melted part of the high melting wire separates two liquid molten pools, and then forms a mechanical interlocking interface between the dissimilar-metal materials.

2.1 Materials

A 7075-aluminum alloy plate with a size of 100 mm×20 mm ×5 mm was selected as the substrate material. The wire material was 304-stainless steel with a diameter of 1.0 mm. Table 1 lists the chemical composition. Before the experiment, the surface of the substrate was polished with 800-grit sandpaper and then cleaned with acetone solution via ultrasonic oscillation to ensure that the base surface was clean.

2.2 Characterization

During the experiments, a Chronos1.4 high-speed camera
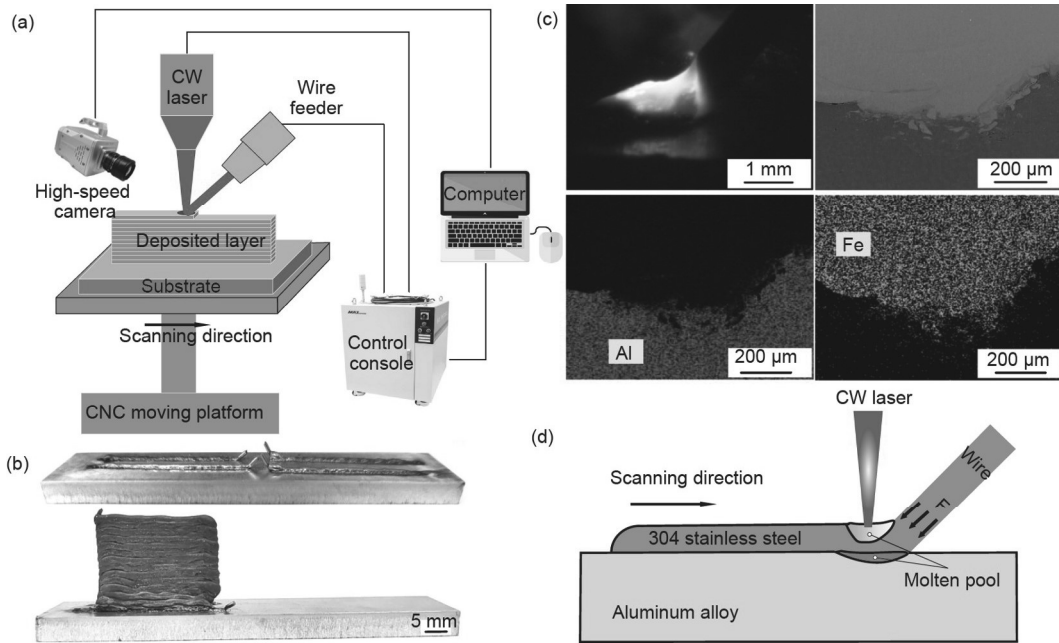
Figure 1 (Color online) Schematic of the laser additive manufacturing for the dissimilar aluminum alloy and stainless steel. (a) Experimental device; (b) single-layer and multilayer samples; (c) microscopic characterization; (d) schematic of DMPIIM.

Table 1 Chemical composition of the dissimilar metals aluminum alloy and stainless steel (wt%)

Element	Zn	Mg	Cu	Mn	Ti	Cr	Si	C	Ni	Fe	Al
7075 aluminum alloy	5.70	2.70	1.50	0.20	0.03	0.20	0.18	–	–	0.36	Bal
304 stainless steel	–	–	–	1.88	–	18.32	0.52	0.09	8.50	Bal	–

(Kron Technologies, Canada) was used to observe the state of the molten track and the condition of the molten pool. After the experiments, the surface topography of samples was observed using a 3D profiler. A wire-cut machine was used to cut the samples to reveal the microstructure of the samples. The cross-section of these samples was polished to a mirror-like surface using 400-, 800-, 1000-, 1500-, and 2000-grit SiC-grinding papers, followed by polishing with 2.5-μm diamond suspension. SEM (Tescan, The Czech Republic) was used to observe the microstructure of the molten track. The elemental composition of the melt track was analyzed by EDS using the line and area scanning models. XRD (Haoyuan Instrument, China) (Cu-Kα: 40 kV, 40 mA) with a scan speed of 2°/min was used to examine the phase and microstructures. The change in the hardness of samples was analyzed using a microhardness tester (HV-1000Z); the holding time and load were 10 s and 300 g, respectively. The formation mechanism of the dissimilar-metal interface was done under the control of an added force simulated using molecular dynamics simulations.

A 3D numerical model of the interaction between dissimilar metals, aluminum alloys, and stainless steel, was established to predict the heat and mass transfer during the LAM process [37]. The implicit successive over relaxation (SOR) and volume of fluid (VOF) algorithms were used to calculate and reconstruct the free surface in the wire-feed LAM of dissimilar metals [38]. The details of the model are given in the Supplementary information. Table 2 lists the material properties of the 7075 aluminum alloy and 304 stainless steel used.

3 Results and discussion

3.1 Effect of the initial contact force

Figure 2 shows the molecular dynamics results of dissimilar-metal molten pools with and without the initial contact force. In the absence of an initial contact force, the diffusion of aluminum atoms was slow, and only some aluminum atoms entered the stainless steel (Figure 2(a-1)). After adding the initial contact force, the aluminum atoms cross the boundary and enter the stainless steel region (Figure 2(b-1)), indicating that the diffusion of aluminum atoms is faster under the action of the initial contact force, which can eventually result in interlocking and stronger mechanical bonding between the dissimilar metals aluminum alloy and stainless steel. Figure 2(a-2) and (b-2) show the temperature curve of the molten pool area of the dissimilar metals with and without initial contact force. The temperature of the molten pool area does not considerably change with or without an initial contact

Table 2 Material properties of the 7075 aluminum alloy and 304 stainless steel [39,40]

| Property	7075 aluminum alloy	304 stainless steel
Density of liquid metal (kg/m^3)	2805	7200
Dynamic viscosity (kg/(m s))	1.25×10^{-3}	6×10^{-3}
Solidus temperature (K)	933	1697
Liquidus temperature (K)	946.3	1727
Specific heat of solid (J/(kg K))	1084	712
Specific heat of liquid (J/(kg K))	997	837
Effective thermal conductivity of solid (W/(m K))	185	19.2
Surface tension (N/m)	0.868	1.76
Temperature coefficient of surface tension (N/(m K))	-3.5×10^{-4}	-4×10^{-4}
Coefficient of thermal expansion (K^{-1})	2.34×10^{-5}	1.72×10^{-5}
Latent heat (J/kg)	3.95×10^5	2.74×10^5

force, indicating that the additional initial contact force would not affect the temperature of the molten pool of dissimilar metals. An initial contact force was applied in the subsequent experiments.

3.2 Process parameters

The dissimilar-metal LAM process was divided into the following four cases based on the interface connection of aluminum alloy substrate and stainless steel wire: case 1, track discontinuity; case 2, poor connection; case 3, interlocked interface; and case 4, excessive heat input. The results of the experimental investigation on the matching relationship between laser power, wire-feed speed, and platform moving speed are shown in Table 3. First, the influence of laser power or wire-feed speed on the interface bonding performance of single-layer molten track was examined by maintaining the platform moving speed at 10 mm/s and changing the laser power and wire-feed speed. The influence of the platform moving speed on the interface bonding performance of the single-layer molten track was then examined, keeping the laser power and wire-feed speed at 660 W and 55 mm/s, respectively.

Table 3 shows that the interface connection between the aluminum alloy substrate and the stainless steel wire has a matching relationship with the laser power, wire-feed speed, and platform moving speed. When the laser power was excessively low, the stainless steel wire was not completely melted but only melted on the top of the wire, and the bonding interface between the aluminum alloy substrate and the stainless steel wire remained solid, thus resulting in poor connection performance. When the laser power was excessively high, the stainless steel wire was completely melted, and many spatters were generated, making it easy to form various IMCs. When the wire-feed speed was excessively fast, the laser could not quickly melt the wire; when
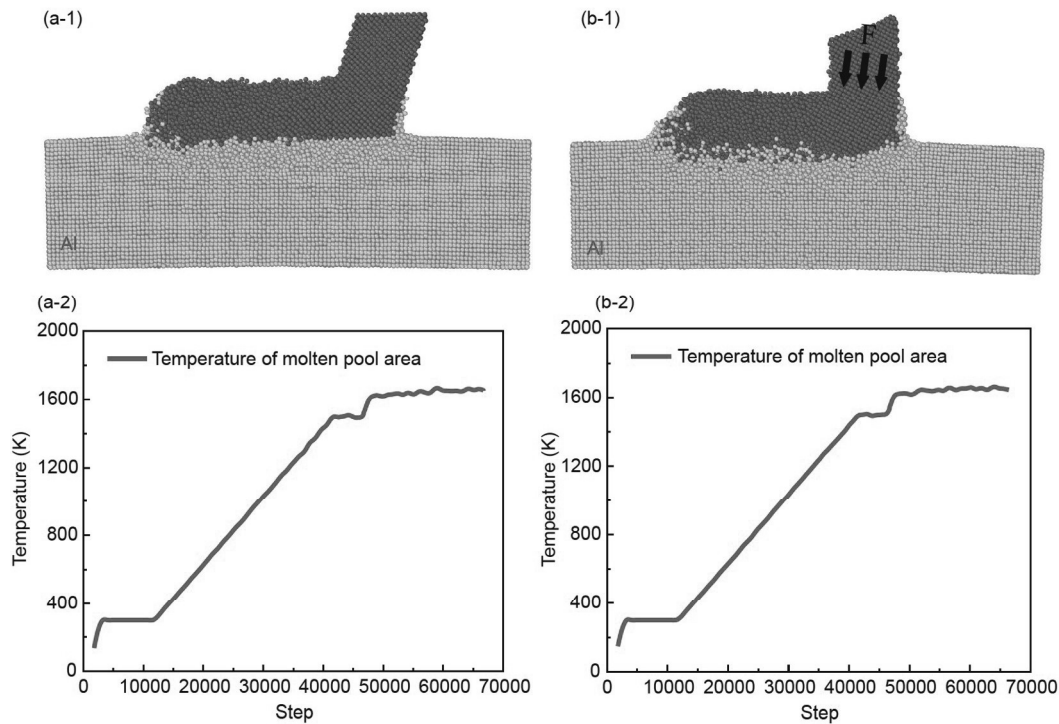
Figure 2 (Color online) Molecular dynamics simulation of the interface formation between aluminum alloy and stainless steel without (a) and with (b) an initial contact force.

Table 3 Processing parameters and connection performance of the experiment

Laser power P (W)	Wire-feed speed V_f (mm/s)	Platform moving speed V_p (mm/s)	Connection performance	Case
400	50	10	Too low energy input	– a)
400	55	10		
500	50	10		
500	55	10	Track discontinuity	Case 1
500	60	10		
600	50	10		
600	55	10		
600	60	10	Poor connection	Case 2
650	50	10		
660	55	11		
660	55	12		
660	54	10		
660	55	10	Interlocked interface	Case 3
650	53	10		
700	50	10		
700	55	10		
700	60	10		
670	50	10		
660	50	10	Excessive heat input	Case 4
660	52	10		
660	53	10		
660	55	8		
660	55	9		

a) "–" means none.

the wire-feed speed was excessively slow, the wire was completely melted, resulting in poor connections. When the platform moved excessively fast or slowly, it caused rapid heat dissipation or accumulation, affecting the connection status. A good connection status was achieved only when the laser power, wire-feed speed, and platform moving speed matched.

The process parameters of four typical cases were selected for the following research. In case 1, the P was 500 W, the V_f was 55 mm/s, and the V_p was 10 mm/s. In case 2, the P was 600 W, the V_f was 55 mm/s, and the V_p was 10 mm/s. In case 3, the P was 660 W, the V_f was 55 mm/s, and the V_p was 10 mm/s. In case 4, the P was 700 W, the V_f was 55 mm/s, and the V_p was 10 mm/s.

3.3 Morphology analysis of samples in the additive manufacturing process

Figure 3 shows a high-speed camera monitoring the LAM process of dissimilar-metal aluminum alloy and stainless steel in different cases. The molten track was discontinuous during the additive manufacturing process. The stainless steel wire was melted only at the top, and its bonding with the aluminum alloy substrate was poor (Figure 3(a)). This observation can be attributed to the laser power being excessively low, causing the stainless steel wire to melt only at the top and transfer less heat to the bottom of the wire. The laser power did not match the platform and wire-feed speeds, thus resulting in a discontinuous molten track and a weak combination of the stainless steel wire and the aluminum alloy substrate. Figure 3(b) shows that, as the laser power increased, most of the stainless steel wire began to melt, the aluminum alloy substrate was melted by heat transfer, and the shape of the molten pool became larger. Compared with Figure 3(b), the molten pool in Figure 3(c) was smaller. Figure 3(d) shows that the entire additive manufacturing process produced significant splashes. This result was attributed to the laser power being excessively high. The excessive heat input caused the stainless steel wire to melt and mix completely [41,42].

Figure 4 shows the samples and 3D profile of the molten track for wire-feed additive manufacturing of dissimilar-metal aluminum alloy and stainless steel in different cases. The figure shows that the molten track in case 1 was discontinuous, and the surface undulation was more severe than in the other cases. Case 2 had a continuous molten track and a
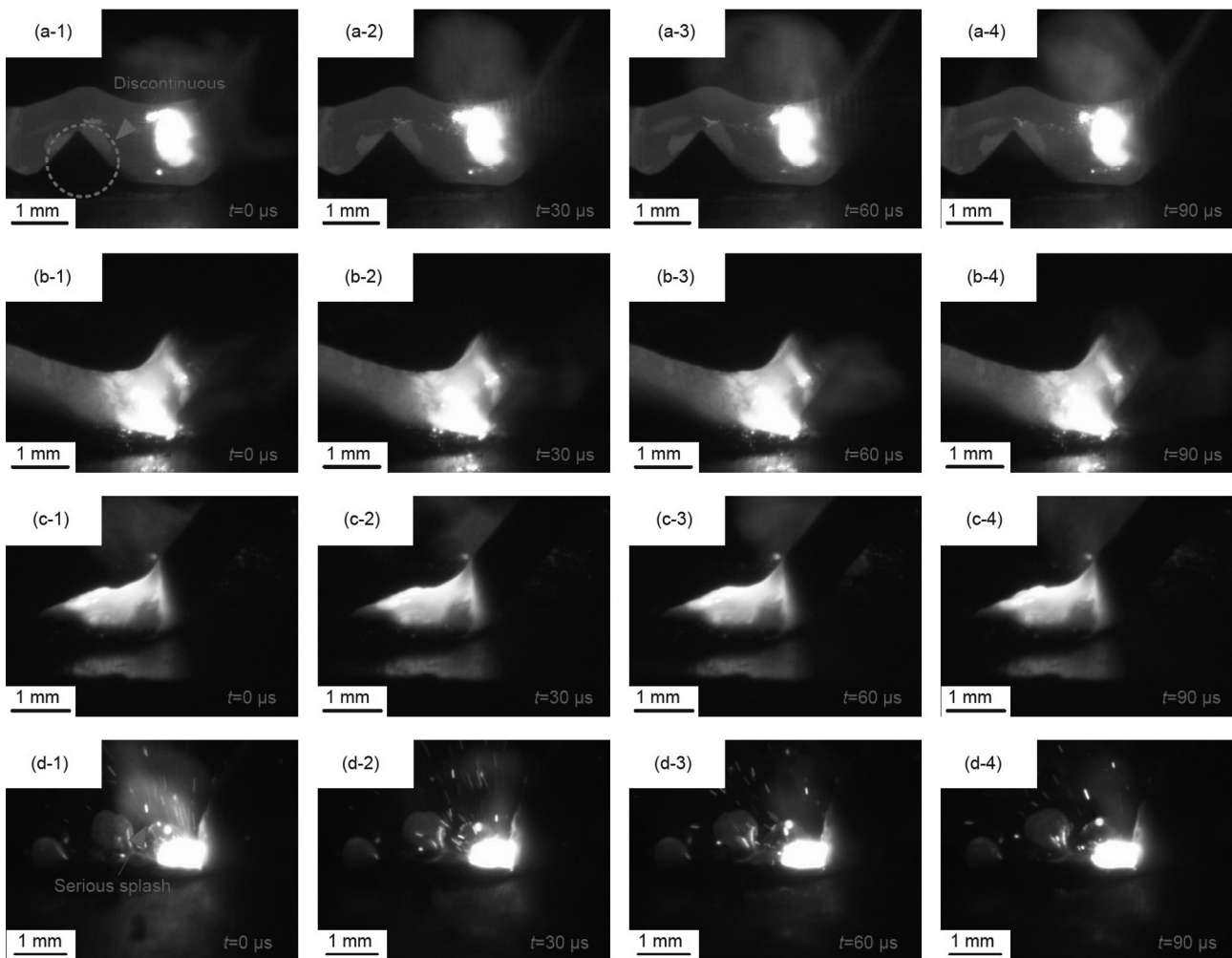
Figure 3 (Color online) Process monitoring with a high-speed camera. (a) Case 1; (b) case 2; (c) case 3; (d) case 4.

high height, and the solidified track could be peeled off easily with pliers. Case 3 had a wider molten track and the best surface morphology, and the molten track could not be peeled off with pliers. Case 4 had the most spatter because the stainless steel was melted completely into the aluminum alloy substrate.

3.4 Microstructure analysis

Figure 5 shows SEM and EDS images of the molten track. The bonding conditions of the molten track interface under four cases (laser powers of 500, 600, 660, and 700 W) are obtained. The line scan result in Figure 5(a-4), (b-4), (c-4), and (d-4) is the position of the black line in Figure 5(a-1), (b-1), (c-1), and (d-1).

Figure 5(a-1) shows that the stainless steel does not completely melt because of the low laser power and insufficient heat input. The joint surface was straight, and there were defects in the bonding surface. Most of the stainless

steel wire melted as the laser power was increased (Figure 5 (b-1)). However, the heat transferred to the aluminum alloy substrate remained low, resulting in an uneven undulation of the joint surface, which was approximately arc-shaped. Moreover, needle-like structures grew from the stainless steel to the aluminum alloy substrate [18]. When the laser power was 660 W, the stainless steel wire melted more (Figure 5(c-1)), and the heat transferred to the aluminum alloy substrate was sufficient to melt the aluminum alloy, thus forming a good bonding surface with a circular arc shape. The Al alloy substrate melted deeper and many cracks appeared (Figure 5(d-1)), indicating that excessive heat input could cause the formation of thermal cracks, which would result in weak interface bonding and easy damage.

The interface between Al and Fe was obvious in the EDS images (Figure 5(a-2), (a-3), and (a-4)); Al was on the aluminum alloy substrate side, and Fe was primarily on the stainless steel side, indicating that there was no apparent IMC layer formation at the interface. The EDS diagrams in
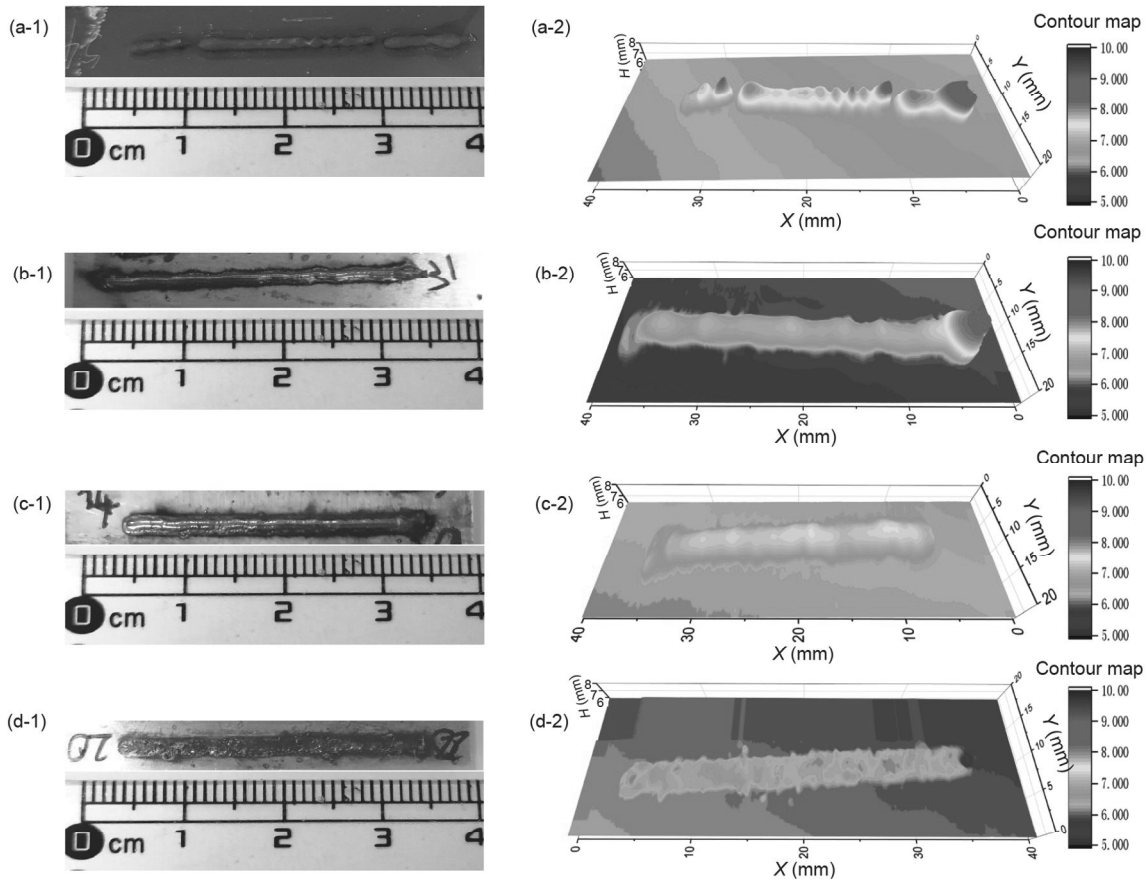
Figure 4 (Color online) Surface topography of the different cases. (a) Case 1; (b) case 2; (c) case 3; (d) case 4. 1, samples; 2, 3D profile.

Figure 5(b-2), (b-3), and (b-4) showed that the Fe in the stainless steel tended to diffuse into the aluminum alloy substrate. Fe in the stainless steel began to precipitate into the aluminum alloy substrate (Figure 5(c-2), (c-3), and (c-4)). During this period, no prominent IMC layer formed at the interface, indicating that the DMPIIM could reduce the formation of an IMC layer under appropriate process parameters. Significant element mixing was observed, as shown in Figure 5(d-2), (d-3), and (d-4), indicating the formation of IMCs [18].

The feature sizes of the molten track, such as the molten pool width (W), molten pool height (H), and molten pool depth (D), were measured (Figure 6), and the corresponding aspect ratio (W/H) of the molten track was calculated under different process parameters. A comparison of the feature sizes of cases 1–4 demonstrated that the width of the molten pool increased as the laser power increased. However, as the height of the molten pool decreased; the depth of the molten pool increased and the aspect ratio of the molten pool increased. When the laser power was 660 W, the wire feeding speed was 55 mm/s, the platform moving speed was 10 mm/s, and the molten track had a good feature size.

The binary phase diagram of Fe-Al [43] in Figure 7(a)

shows that the IMCs can be Fe_3Al, $FeAl$, $FeAl_2$, Fe_2Al_5, and $FeAl_3$. By combining the XRD and EDS results [26,44], Fe_3Al and $FeAl$ IMCs were formed. In case 1, the input heat was small. No notable IMCs were generated. In other cases, the molten liquid Al on the aluminum alloy substrate diffused into the undissolved solid Fe in the stainless steel wire to form Fe_3Al, but there was no obvious IMC layer caused by the existence of a double molten pool. And as the heat input increased, the content of Al in Fe increased, resulting in the formation of FeAl compounds with high content.

3.5 Microhardness

The joint properties of dissimilar-metal aluminum alloys and stainless steels were characterized using microhardness [43]. The Vickers hardness test was performed on the cross-section of the sample (Figure 8(a)). The test direction was along the direction of the deposition height, and the testing was done every 200 μm.

Figure 8(b) showed that the hardness value of the aluminum alloy side ranged from 141 to 190 HV and that the hardness of the aluminum alloy side did not change significantly in different cases. A minor difference was noted in
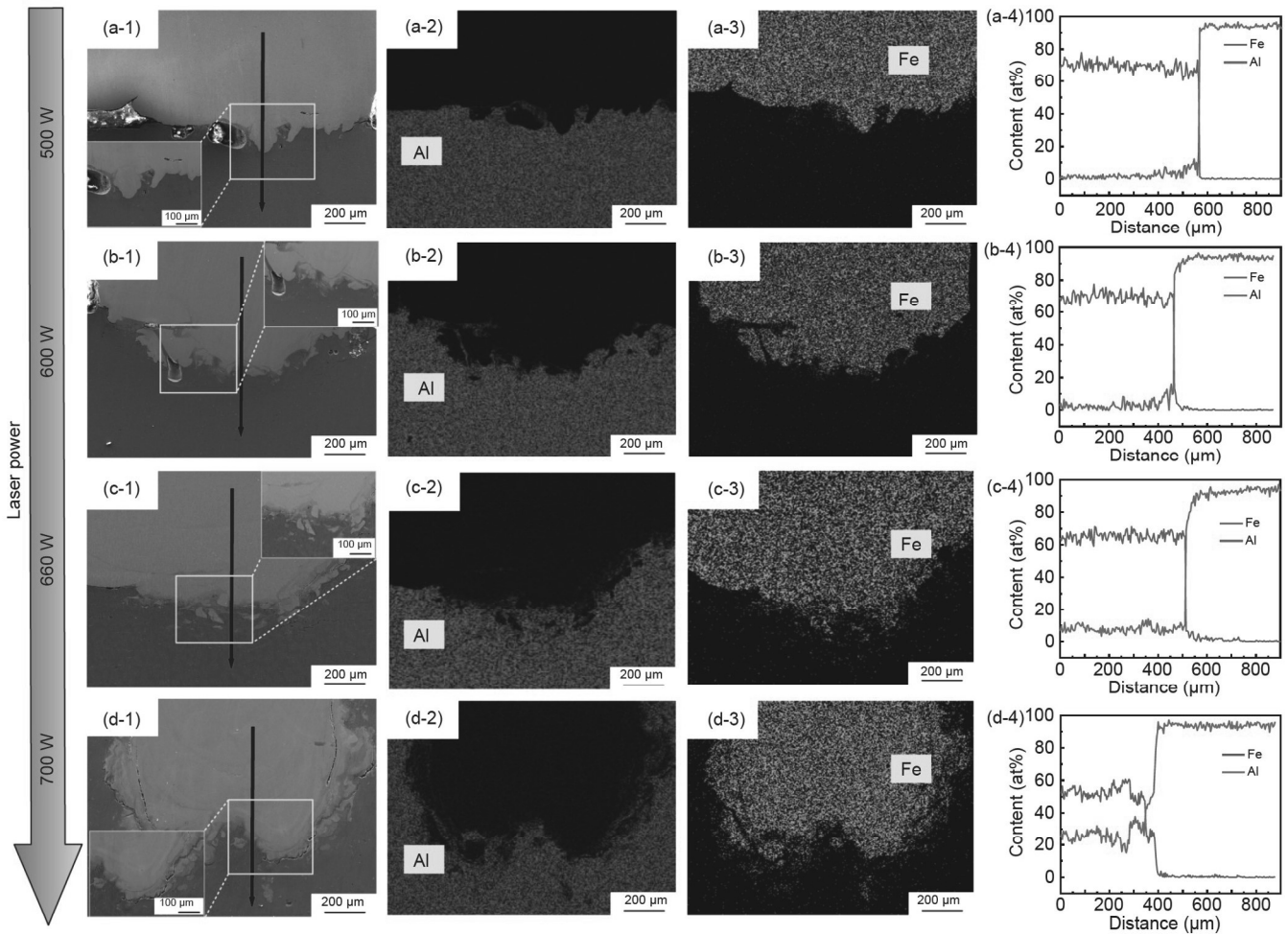
Figure 5 (Color online) SEM and EDS images in different cases. (a) Case 1; (b) case 2; (c) case 3; (d) case 4.

the hardness value at the interface under different cases. In case 1, the stainless steel side had the lowest hardness. In the other three cases, the hardness increased from the interface to the stainless steel side because of the rapid solidification of the stainless steel wire [45]. In case 3, when the heat input was 660 W, the stainless steel side had the highest hardness compared to that in cases 1, 2, and 4. The top of the stainless steel wire was fully melted, and the structure was uniform, thus resulting in finer dendritic primary arm length under rapid cooling [27,46].

3.6 Simulation of interface formation

Figure 9 shows the temperature fields of the dissimilar metals joining in different cases. The velocity vectors of the melt flow were represented with black arrows in each image. The validity of the 3D numerical model was experimentally confirmed. Figure 9(a-2), (b-2), (c-2), and (d-2) showed that as the laser power increased, the molten pool height decreased, the width increased, and the depth increased, which was consistent with the data measured in the experiment

(Figure 6). When the heat input was low, the stainless steel wire was only partially melted, and a discontinuity appeared at the interface connection (Figure 9(a-1)). This result is consistent with the phenomenon observed in the experiment shown in Figure 3.

4 Conclusions

The wire-feed LAM directed energy deposition technology based on the proposed DMPIIM was used to produce single-layer and multilayer samples of dissimilar-metal aluminum alloy and stainless steel. This study investigated the bonding ability of the single-layer molten track in different cases. The primary conclusions of the study are summarized as follows.

(1) Through molecular dynamics simulations, the diffusion rate of aluminum atoms in the aluminum alloy substrate to the stainless steel was faster under the action of the initial contact force than that without the initial contact force. The added initial contact force would not affect the temperature of the dissimilar-metal aluminum alloy and stainless steel
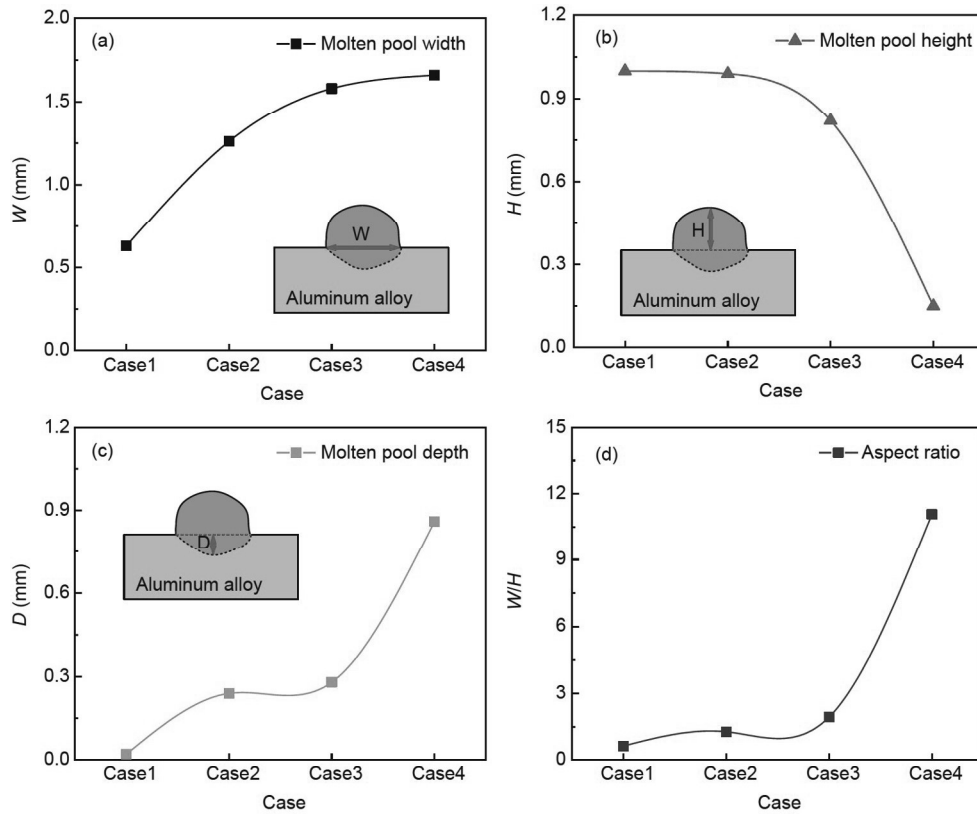
Figure 6 (Color online) Feature size of the molten track. (a) Molten pool width; (b) molten pool height; (c) molten pool depth; (d) aspect ratio.
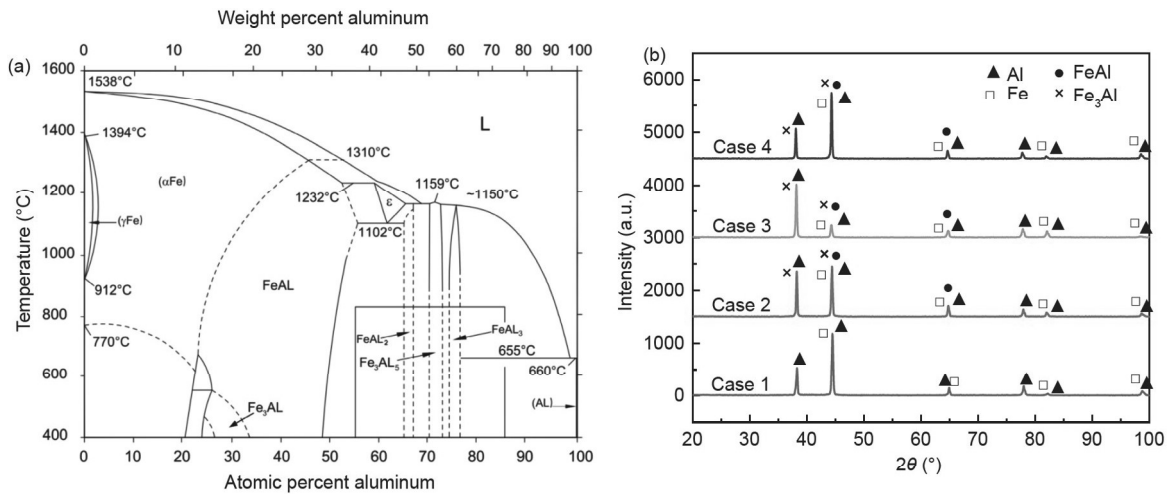

Figure 7 (Color online) (a) Fe-Al binary phase diagram; (b) XRD results of different cases.

molten pool.

(2) The preferred process parameters of the dissimilar-metal aluminum alloy and stainless steel DMPIIM process were obtained, and a matching relationship between the interface connection of dissimilar-metal aluminum alloy and stainless steel and the process parameters (laser power, wire-feed speed, and platform moving speed) was established.

(3) When the laser power was 660 W, the wire feeding

speed was 55 mm/s, and the platform moving speed was 10 mm/s, the interface of dissimilar metals was the best and could not be peeled off, and it had good feature size and microhardness. SEM and XRD demonstrated excellent mechanical occlusion at the connection interface and no obvious IMC layer.

This study provides an important reference for future research in dissimilar-metal aluminum alloy and stainless steel
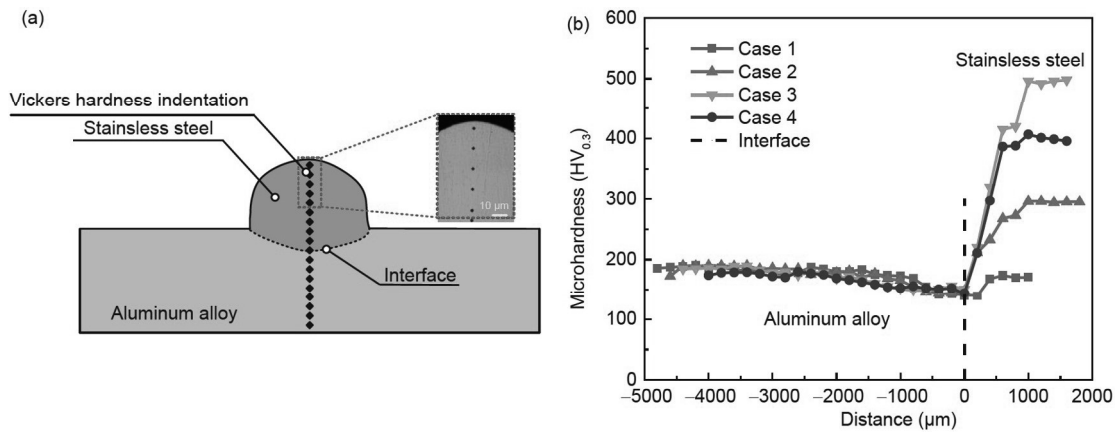
Figure 8 (Color online) Microhardness results of dissimilar metals aluminum alloy and stainless steel laser additive manufacturing process in different cases. (a) Schematic of microhardness points; (b) microhardness distribution curve.
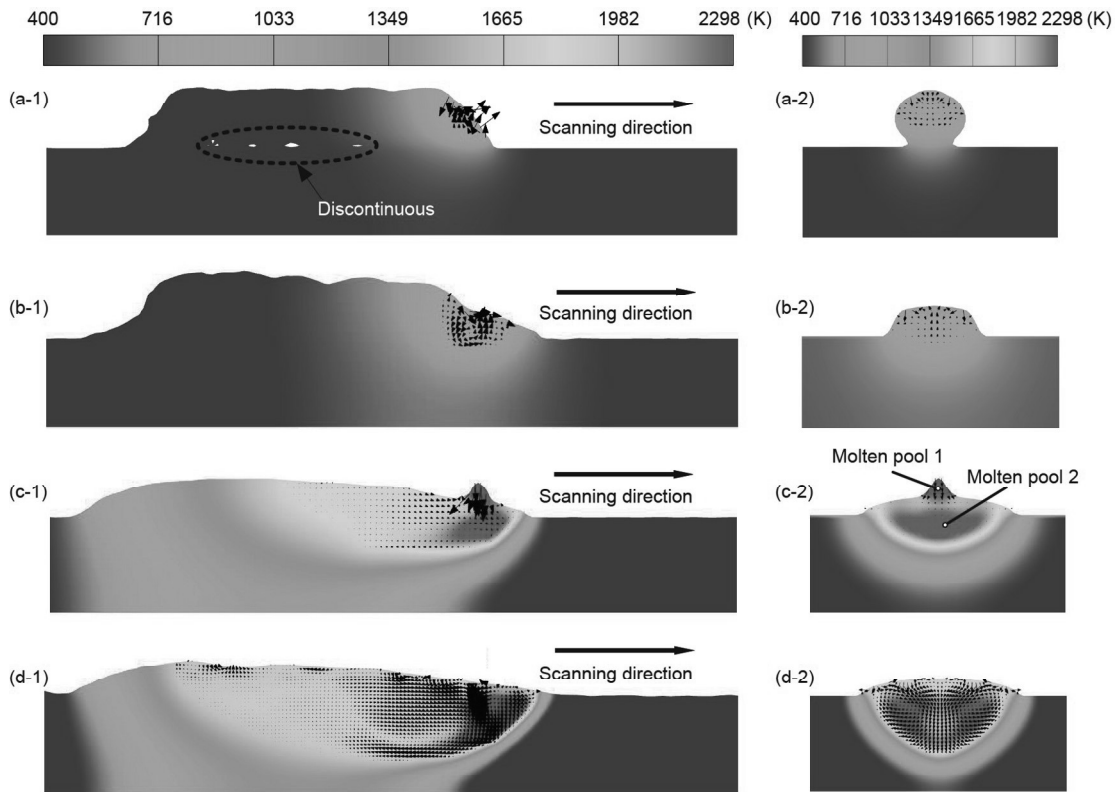
Figure 9 (Color online) Evolution of the temperature fields in the different cases. (a) Case 1; (b) case 2; (c) case 3; (d) case 4. 1-longitudinal section; 2-cross section.

wire-feed LAM. The DMPIIM can effectively reduce the IMC layer when dissimilar metals need to be connected in the aerospace field.

1 Li Q, Xu C, Gao S, et al. Research on the forming quality of clinched joint for dissimilar sheet metal. Int J Adv Manuf Technol, 2022, 119: 2945–2959

2 Zhang C, Gou R, Yu M, et al. Mechanical and fatigue properties of self-piercing riveted joints in high-strength steel and aluminium alloy. J Iron Steel Res Int, 2017, 24: 214–221

3 Liu X, Lan S, Ni J. Analysis of process parameters effects on friction stir welding of dissimilar aluminum alloy to advanced high strength

steel. Mater Des, 2014, 59: 50–62

4 Simar A, Avettand-Fènoël M N. State of the art about dissimilar metal friction stir welding. Sci Tech Welding Joining, 2017, 22: 389–403

5 Hu Y, He X, Yu G, et al. Heat and mass transfer in laser dissimilar welding of stainless steel and nickel. Appl Surf Sci, 2012, 258: 5914–5922

6 Wang Y L, Jiang P, Geng S N, et al. Spatial distribution of laser energy and its influence on the stability of extreme narrow keyholes during ultra-high power laser welding. Sci China Tech Sci, 2022, 65: 2079–2088

7 Chen X, Su C, Wang Y, et al. Cold metal transfer (CMT) based wire and arc additive manufacture (WAAM) system. J Surf Invest, 2018, 12: 1278–1284

8 Wu Q, Lu J, Liu C, et al. Obtaining uniform deposition with variable wire feeding direction during wire-feed additive manufacturing. Mater Manufacturing Processes, 2017, 32: 1881–1886

9 Liu J, Zhao S, Zhang X, et al. A laser-shock-enabled hybrid additive manufacturing strategy with molten pool modulation of Fe-based alloy. J Manufacturing Processes, 2022, 82: 657–664

10 Khodabakhshi F, Farshidianfar M H, Bakhshivash S, et al. Dissimilar metals deposition by directed energy based on powder-fed laser additive manufacturing. J Manufacturing Processes, 2019, 43: 83–97

11 Ding D, Pan Z, Cuiuri D, et al. Wire-feed additive manufacturing of metal components: Technologies, developments and future interests. Int J Adv Manuf Technol, 2015, 81: 465–481

12 Ramalho A, Santos T G, Bevans B, et al. Effect of contaminations on the acoustic emissions during wire and arc additive manufacturing of 316L stainless steel. Additive Manufacturing, 2022, 51: 102585

13 Wang P, Chen X, Pan Q, et al. Laser welding dissimilar materials of aluminum to steel: An overview. Int J Adv Manuf Technol, 2016, 87: 3081–3090

14 Huang W, Chen S, Xiao J, et al. Laser wire-feed metal additive manufacturing of the Al alloy. Optics Laser Tech, 2021, 134: 106627

15 Abioye T E, Medrano-Tellez A, Farayibi P K, et al. Laser metal deposition of multi-track walls of 308LSi stainless steel. Mater Manufacturing Processes, 2017, 32: 1660–1666

16 Gockel J, Beuth J, Taminger K. Integrated control of solidification microstructure and melt pool dimensions in electron beam wire feed additive manufacturing of Ti-6Al-4V. Additive Manufacturing, 2014, 1-4: 119–126

17 Cheng K, Zhang M B, Song H, et al. Additive manufacturing of Ti-6Al-4V alloy by hybrid plasma-arc deposition and microrolling: Grain morphology, microstructure, and tensile properties. Sci China Tech Sci, 2022, 65: 849–857

18 Sun H, Chu X, Luo C, et al. Selective laser melting for joining dissimilar materials: Investigations of interfacial characteristics and *in situ* alloying. Metall Mater Trans A, 2021, 52: 1540–1550

19 Syed W U H, Pinkerton A J, Li L. A comparative study of wire feeding and powder feeding in direct diode laser deposition for rapid prototyping. Appl Surf Sci, 2005, 247: 268–276

20 Yang J, Oliveira J P, Li Y, et al. Laser techniques for dissimilar joining of aluminum alloys to steels: A critical review. J Mater Processing Tech, 2022, 301: 117443

21 Xia H, Tao W, Li L, et al. Effect of laser beam models on laser welding-brazing Al to steel. Optics Laser Tech, 2020, 122: 105845

22 Sadmai K, Kaewwichit J, Roybang W, et al. Microstructure and tensile strength of butt joint between AA6063 aluminum alloy and AISI304 stainless steel by friction stir welding. Int J Adv Culture Tech, 2015, 3: 179–187

23 Sun J, Yan Q, Gao W, et al. Investigation of laser welding on butt joints of Al/steel dissimilar materials. Mater Des, 2015, 83: 120–128

24 Yang J, Li Y, Zhang H. Microstructure and mechanical properties of pulsed laser welded Al/steel dissimilar joint. Trans Nonferrous Met Soc China, 2016, 26: 994–1002

25 Pouranvari M. Critical assessment 27: Dissimilar resistance spot welding of aluminium/steel: Challenges and opportunities. Mater Sci Tech, 2017, 33: 1705–1712

26 Movahedi M, Kokabi A H, Reihani S M S, et al. Effect of tool travel and rotation speeds on weld zone defects and joint strength of aluminium steel lap joints made by friction stir welding. Sci Tech Welding Joining, 2012, 17: 162–167

27 Madhavan S, Kamaraj M, Vijayaraghavan L, et al. Microstructure and mechanical properties of aluminium/steel dissimilar weldments: effect of heat input. Mater Sci Tech, 2017, 33: 200–209

28 Zhao Y, Long Y, Li Z. Research progress of transition layer and filler wire for laser welding of steel and aluminum dissimilar metals. Int J Adv Manuf Technol, 2022, 119: 4149–4158

29 Tey C F, Tan X, Sing S L, et al. Additive manufacturing of multiple materials by selective laser melting: Ti-alloy to stainless steel via a Cu-alloy interlayer. Additive Manufacturing, 2020, 31: 100970

30 Pardal G, Ganguly S, Williams S, et al. Dissimilar metal joining of stainless steel and titanium using copper as transition metal. Int J Adv Manuf Technol, 2016, 86: 1139–1150

31 Yu G, Zou T, Chen S, et al. Effect mechanism of Ni coating layer on the characteristics of Al/steel dissimilar metal brazing. Mater Charact, 2020, 167: 110518

32 Chen S, Huang J, Ma K, et al. Influence of a Ni-foil interlayer on Fe/Al dissimilar joint by laser penetration welding. Mater Lett, 2012, 79: 296–299

33 Song T F, Jiang X S, Shao Z Y, et al. Microstructure and mechanical properties of vacuum diffusion bonded joints between Ti-6Al-4V titanium alloy and AISI316L stainless steel using Cu/Nb multi-interlayer. Vacuum, 2017, 145: 68–76

34 Shang C, Wang C, Xu G, et al. Laser additive manufacturing of TA15 - Inconel 718 bimetallic structure via Nb/Cu multi-interlayer. Vacuum, 2019, 169: 108888

35 Li Y, Shen Y, Hung C H, et al. Additive manufacturing of Zr-based metallic glass structures on 304 stainless steel substrates via V/Ti/Zr intermediate layers. Mater Sci Eng-A, 2018, 729: 185–195

36 Li W, Karnati S, Kriewall C, et al. Fabrication and characterization of a functionally graded material from Ti-6Al-4V to SS316 by laser metal deposition. Additive Manufacturing, 2017, 14: 95–104

37 Lu H, Zhang X, Liu J, et al. Study on laser shock modulation of melt pool in laser additive manufacturing of FeCoCrNi high-entropy alloys. J Alloys Compd, 2022, 925: 166720

38 Lu H, He Y, Zhao Z, et al. Strengthening CoCrFeNi high entropy alloys via additive manufacturing with laser shock modulation of melt pool. Mater Sci Eng-A, 2022, 860: 144295

39 Wang L, Zhang Y, Yan W. Evaporation model for keyhole dynamics during additive manufacturing of metal. Phys Rev Appl, 2020, 14: 064039

40 Du J, Wang X, Bai H, et al. Numerical analysis of fused-coating metal additive manufacturing. Int J Thermal Sci, 2017, 114: 342–351

41 Yang J, Hu A, Li Y, et al. Heat input, intermetallic compounds and mechanical properties of Al/steel cold metal transfer joints. J Mater Processing Tech, 2019, 272: 40–46

42 Wang C, Cui L, Mi G, et al. The influence of heat input on microstructure and mechanical properties for dissimilar welding of galvanized steel to 6061 aluminum alloy in a zero-gap lap joint configuration. J Alloys Compd, 2017, 726: 556–566

43 Nguyen V, Nguyen Q, Huang S C. Microstructure and mechanical properties of butt joints between stainless steel SUS304l and aluminum alloy A6061-T6 by TIG welding. Materials, 2018, 11: 1136

44 Yang Y. Laser welding of dissimilar metal of aluminium and steel (in Chinese). Dissertation for the Master's Degree. Changchun: Changchun University of Science and Technology, 2011. 40–41

45 Yasuyama M, Ogawa K, Taka T. Spot welding of aluminium and steel sheet with an insert of aluminium clad steel sheet: Dissimilar metal joining of aluminium and steel sheet (1st Report). Welding Int, 1996, 10: 963–970

46 Chuaiphan W, Srijaroenpramong L. Effect of welding speed on microstructures, mechanical properties and corrosion behavior of GTA-welded AISI 201 stainless steel sheets. J Mater Processing Tech, 2014, 214: 402–408